Characterizing the conformational dynamics of metal-free PsaA using molecular dynamics simulations and electron paramagnetic resonance spectroscopy

Evelyne Deplazes [1,2,‡], *Stephanie L. Begg* [3,‡], *Jessica H. van Wonderen* [4‡], *Rebecca Campbell* [3], *Bostjan Kobe* [1,2,5], *James C. Paton* [3], *Fraser MacMillan* [4], *Christopher A. McDevitt* [3,*], *Megan L. O'Mara* [1,6,*]

[1] School of Chemistry and Molecular Biosciences, The University of Queensland, Brisbane, Australia.

[2] Institute for Molecular Bioscience, The University of Queensland, Brisbane, Australia.

[3] Research Centre for Infectious Diseases, School of Biological Sciences, University of Adelaide, Adelaide, Australia.

[4] Henry Wellcome Unit for Biological EPR, School of Chemistry, Norwich Research Park, University of East Anglia, Norwich, UK

[5] Australian Infectious Diseases Research Centre, University of Queensland, Brisbane, Australia

[6] Research School of Chemistry, The Australian National University, Canberra, Australia.

‡ E.D., S.B. and JHvW contributed equally to this work.

*Corresponding Authors:

Dr. Megan L. O'Mara, E-mail: megan.o'mara@anu.edu.au

Dr. Christopher A. McDevitt, E-mail: christopher.mcdevitt@adelaide.edu.au

ABSTRACT

Prokaryotic metal-ion receptor proteins, or solute-binding proteins, facilitate the acquisition of metal ions from the extracellular environment. Pneumococcal surface antigen A (PsaA) is the primary Mn^{2+}-recruiting protein of the human pathogen *Streptococcus pneumoniae* and is essential for its *in vivo* colonization and virulence. The recently reported high-resolution structures of metal-free and metal-bound PsaA have provided the first insights into the mechanism of PsaA-facilitated metal binding. However, the conformational dynamics of metal-free PsaA in solution remain unknown. Here, we use continuous wave electron paramagnetic resonance (EPR) spectroscopy and molecular dynamics (MD) simulations to study the relative flexibility of the structural domains in metal-free PsaA and its distribution of conformations in solution. The results show that the crystal structure of the metal-free PsaA is a good representation of the dominant conformation in solution, but the protein also samples structurally distinct conformations that are not captured by the crystal structure. The results also suggest that the metal binding site is larger and more solvent exposed than indicated by the metal-free crystal structure. This study provides atomic-resolution insight into the conformational dynamics of PsaA prior to metal binding and lay the groundwork for future EPR and MD based studies of PsaA in solution.

GRAPHICAL ABSTRACT

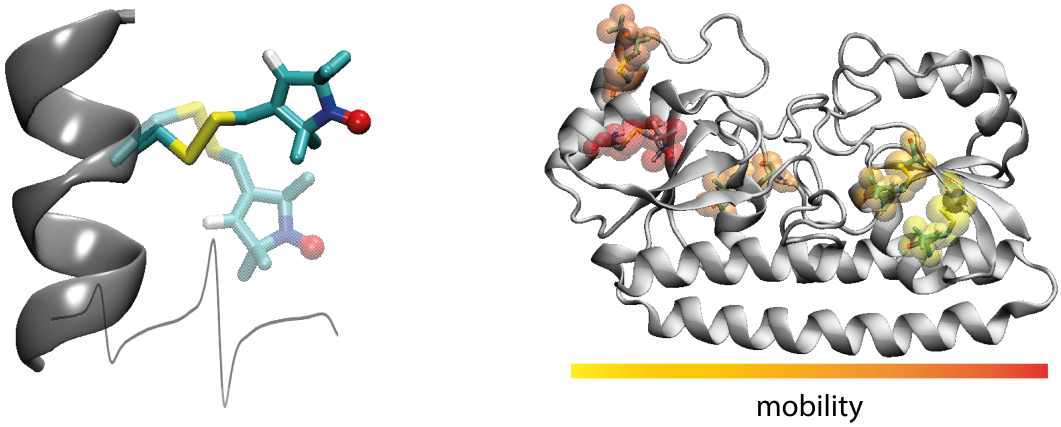

HIGHLIGHTS

- PsaA is the Mn^{2+}-recruiting protein of the human pathogen *Streptococcus pneumoniae*
- Metal-free PsA samples structurally distinct conformations not captured by the crystal structure
- The metal binding site is larger and more solvent exposed than indicated by the crystal structure

KEYWORDS

Cluster A-I solute-binding protein (SBP); *S*treptococcus pneumoniae; PsaA; molecular dynamics simulations, electron paramagnetic resonance (EPR) spectroscopy; protein flexibility; spin-label mobility, Pneumococcal surface antigen A, protein conformations

INTRODUCTION

Metal-ion receptor proteins in prokaryotic cells represent a functional dichotomy. They bind metal ions from the extracellular environment with nanomolar affinity via thermodynamically favourable interactions between the ion and the binding site in the protein [1, 2]. However, efficacious scavenging of ions relies upon the subsequent release of the ion from the binding site to facilitate transport into the cell. This combination of high-affinity binding followed by ligand release enables cellular accumulation of metal ions from the extracellular space, which is essential for a range of intracellular processes [3, 4]. Despite this, the metal-free conformations of metal-ion receptor proteins have been poorly characterized due to the intrinsic challenge of isolating them without contamination by co-purifying metal ions.

Pneumococcal surface antigen A (PsaA) is the essential Mn^{2+}-recruiting protein of the major human pathogen *Streptococcus pneumoniae*, which is a causative agent of bacterial pneumonia, meningitis, septicaemia and otitis media [5, 6]. Manganese has crucial roles in *S. pneumoniae*, including in the protection against superoxide stress, in capsule production, and in metabolism. As a consequence, impairment of the Psa permease attenuates *in vivo* virulence of *S. pneumoniae* [5, 7-10]. In addition to its role in metal acquisition, the P4 region (residues 251-278) of PsaA is immunogenic [11-13]. The P4 region has also been implicated in mediating PsaA adhesion to nasopharyngeal epithelial cells [9-14], although the *in vivo* relevance of this adhesin property remains contentious. *S. pneumoniae* is the foremost bacterial pathogen associated with mortality in children less than 5 years old worldwide [15]. The reduced efficacy of current vaccine regimes, together with the spread of multidrug resistant strains, highlights an urgent need to develop new therapeutic strategies for the management of pneumococcal infections [16]. Due to the central role of PsaA in the establishment of *S. pneumoniae* infections, understanding how the structure and conformational dynamics of PsaA is related to its physiological function can form an important contribution to the development of new strategies to prevent and treat pneumococcal disease.

PsaA belongs to the Cluster A-I subgroup of solute-binding proteins (SBPs) associated with ABC permeases. It has a two-lobed organization comprising of N- and C-terminal $(\beta/\alpha)_4$-domains linked by a rigid helix, and bisected by a cleft in which the Mn^{2+} ion binds [17, 18] (Figure 1a). This overall fold is conserved amongst SBPs in the cluster A group that interact directly with metal ions [16, 19], or bind chelated metals [20] or vitamins [21]. Recent structural advances have revealed that the length and flexibility of the linking helix in the SBPs plays a crucial role in the mechanism of ligand binding. The role of the linking helix is well defined in cluster B SBPs, such as the amino acid binding SBP LivJ, which has a considerably shorter helical linker region permitting large domain movements (up to 60°) upon ligand binding. This ligand binding mechanism in cluster B SBPs is commonly referred to as a 'Venus flytrap' binding mode [22]. The lack of high-resolution structural information on the conformational landscapes of SBPs from other clusters has precluded conclusions about the generality of this mechanism. Furthermore, the length of the helical linker domain suggested that other SBPs were unlikely to undergo such extensive domain rearrangements.

The recent elucidation of a set of high-resolution structures of metal-free PsaA in the open state enabled the first comparison of the open and closed conformations of the Cluster A-I subgroup of SBPs [23]. Based on these crystal structures, it was proposed that the helical linking region restricts the extent of conformational movement within PsaA. In contrast to the large movements observed in the LivJ structures, the metal-free and metal-bound structures of PsaA only showed a relatively minor (~13°) rotation of the C-terminal domain, in which the pivoting was centered on the last segment of the linking helix (residues 190 -194). As such, this distinct conformational transition, which suggests a relatively rigid protein, was likened to a 'spring-hammer' binding mechanism [23]. However, crystal structures represent static snapshots of proteins, usually captured in a single conformation within the crystal lattice. Consequently, the metal-free PsaA structure represents one stable conformation of the protein, and may not reveal the full extent of conformational dynamics of metal-free PsaA in solution. Therefore, it remains to be ascertained how the crystallographic structure of metal-free PsaA compares to its conformational flexibility in solution. Previous MD

studies of PsaA have examined the structural changes that are induced by removing the metal ion from the metal-bound protein [23]. The series of 50 ns simulations from that work showed that the observed structural changes were consistent with the proposed spring-hammer mechanism [23]. However, they did not converge to the metal-free crystallographic conformation, suggesting that the conformational flexibility of PsaA is greater than suggested by the metal-free and metal-bound crystal structures. Hence, the aim of this study was to combine molecular dynamics (MD) simulations and continuous wave (cw) electron paramagnetic resonance (EPR) spectroscopy to characterize the mobility of the structural domains of metal-free PsaA, and determine the conformations sampled by the protein in the absence of the metal ion. The combined results from EPR spectroscopy and MD simulations show that, while the high-resolution structure of metal-free PsaA is a good representation of the predominant conformation of PsaA in solution, the protein also samples structurally distinct conformations that are not captured by the crystal structure. Furthermore, in all simulations of metal-free PsaA, the metal binding site was more solvent exposed than in the crystal structure. The unwinding of the linking helix, characteristic of all metal-bound structures crystallised thus far, [23] was not observed in our simulations of metal-free PsaA, suggesting that this conformational change is only induced upon metal binding. This study characterizes the intrinsic flexibility of metal-free PsaA in solution, providing additional structural information that cannot be obtained from the available crystal structures. These results contribute to a greater understanding of the structure-function mechanisms of metal-receptor proteins in *S. pneumoniae* and other prokaryotes.

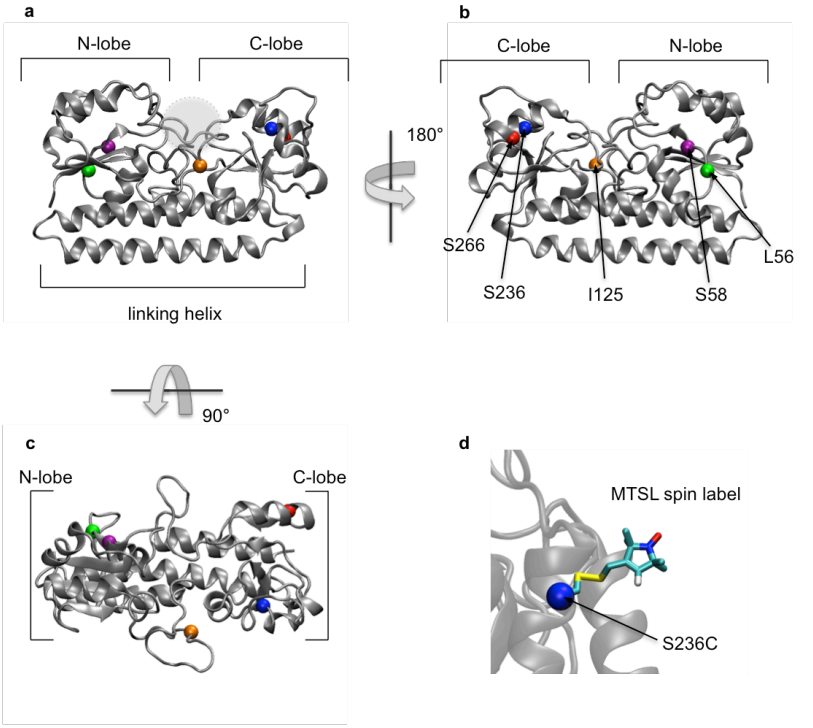

Figure 1. *Structure of metal-free PsaA. The location of the metal binding site is indicated by a shaded circle (a). The Cα atoms of residues that were used for spin-labelling are shown as coloured spheres (a,b,c). In each of the five Cys-PsaA variants the corresponding wild-type residues was replaced by a Cys residue and labelled with MTSL, as shown in the example of residue S236C (d).*

METHODS

Expression and purification of PsaA and variants

Recombinant PsaA was cloned from *S. pneumoniae* D39 genomic DNA, gene SPD_1463, into pCAMcLIC01-PsaA as previously described [18]. The recombinant sequence of PsaA (Supplementary Table 1) is the mature soluble portion of the protein (residues 32-309) and does not contain any endogenous cysteine residues. Site-directed mutagenesis (Quikchange Lightning Kit, Agilent Technologies) was used to introduce the cysteine mutations in the coding sequence of pCAMcLIC01-PsaA to generate Cys-PsaA mutant variants (all primers are listed in Supplementary Table S2). Protein expression was performed in *E. coli* LEMO21(DE3), by growing the cells in an

autoinducing TB medium (Overnight Express, Merck) for 18 hours at 303 K. Cells were harvested and disrupted at 30 kPSI by a Constant Systems cell disruptor and the soluble supernatant isolated by centrifugation at 277 K for 60 min at 120,000 × *g*. PsaA was isolated in a Histrap HP column on an AKTA Purifier and was further purified on a Superdex 200 10/300 gel filtration column (GE Healthcare). The dodecahistidine tag was removed by enzymatic digestion by the human rhinovirus 3C protease and the protein purified further on a Histrap HP column.

Generation of metal-free PsaA

Purified metal-free PsaA and mutant variants were prepared by dialyzing the protein with the polyhistidine-tag removed (10 mL) in a 20 kDa molecular weight cut-off membrane (Pierce) against 4 L of sodium acetate buffer, pH 3.7, with 20 mM EDTA at 300 K. The sample was then dialyzed against 4 L of 20 mM Tris-HCl, pH 7.2, 100 mM NaCl, at 277 K and centrifuged at 18,000 × *g* for 10 min to remove any insoluble material. The Cys-PsaA variants were purified using essentially the same procedure with 5 mM dithiothreitol (DTT) or 5 mM tris(2-carboxyethyl)phosphine (TCEP) included in all buffers. Protein samples were analysed for metal content by heating 10 μM protein at 370 K for 30 min in 3.5% HNO_3. Samples were analysed by inductively-coupled plasma mass spectroscopy (ICP-MS) on an Agilent 7500cx ICP-MS (Adelaide Microscopy, University of Adelaide).

Protein assays

Metal-loading assays were performed on purified metal-free PsaA variants (30 μM) by mixing with 300 μM $MnSO_4$ (10-fold excess) in a total volume of 2 mL into the assay buffer (20 mM MOPS, pH 7.2, 100 mM NaCl) for 60 min at 277 K. The sample was desalted on a PD10 column (GE Healthcare) into the assay buffer and the protein concentration was quantitated. The protein was then analysed by ICP-MS. 5-10 μM solutions of control (metal-free) and metal-loaded protein were prepared in 3.5% HNO_3 and boiled for 30 min at 370 K. Samples were then cooled and centrifuged

for 20 min at 14,000 x *g*. The supernatant was then analysed ICP-MS and the protein-to-metal ratio determined.

Labelling of PsaA variants with MTSL

The Cys-PsaA variants were spin-labelled using the cysteine-specific label MTSL (*S*-(1-oxyl-2,2,5,5-tetramethyl-2,5-dihydro-1H-pyrrol-3-yl)methyl methanesulfonothioate) (Toronto Chemicals). A ~10-fold excess of DTT was added prior to labelling to reduce any disulfide bonds and then removed after 1 hour using a PD-10 column and Chelex-100 treated 20 mM MOPS, pH 7.2, 100 mM NaCl. Samples were then immediately labelled using a 10-fold molar excess of MTSL to PsaA, from a 50 mM MTSL-DMSO stock, and left to react for 3 hours in the dark with mild shaking. Unbound MTSL was removed by buffer exchange (4×) with Chelex-100 treated 20 mM MOPS, pH 7.2, 100 mM NaCl and concentrated using spin concentrators (10 kDa molecular weight cut-off).

Continuous wave electron paramagnetic resonance measurements

Room-temperature X-band cw EPR spectra were acquired using a *Bruker* eleXsys E500 spectrometer fitted with a *Bruker* ER4123D loop-gap resonator. The total active sample volume was 10 µl. Experimental parameters for the cw EPR spectra were: microwave power, 0.6315 mW; field modulation amplitude, 1 G; field modulation frequency, 100 kHz; sweep width, 9 mT; number of scans, 32 scans. The spectra were quantified by double integration against a known concentration of MTSL to give concentrations between 100 to 300 µM MTSL-labelled PsaA, which were comparable to the concentrations calculated by a standard protein assay.

Simulations of the cw-EPR spectra were performed using the program Easyspin[24]. Random rotational motion of the spin probe was assumed, and the corresponding correlation time, τ_c, was an adjustable parameter. All five spectra were simulated using parameters typical for a nitroxide spin probe with $g_z \sim 2$ and A_{zz} =34-38 Gauss. The spectra of the L56C, S58C, I125C

and S266C PsaA variants were simulated using a single component, whereas the spectrum of the I236C PsaA variant required simulation with two components. For the two-component simulation, the τ_c of both components is given.

MD simulations of wild-type and spin-labelled PsaA

All MD simulations were performed using the GROMACS (Groningen Machine for Chemical Simulation) package version 3.3.3 [25], in conjunction with the GROMOS 54A7 force field [26] for proteins. The metal-free PsaA crystal structure (PDB-ID 3ZK7) was used as a starting point for all simulations. The crystallographic water molecules were retained. Water was described using the simple point charge (SPC) water model [27]. All simulations were performed under periodic boundary conditions using a rectangular box with at least 1.2 nm between the protein and the box wall. The van der Waals interactions were evaluated using a 0.8 nm cut-off. To minimize the effect of truncating the electrostatic interactions beyond the 1.4 nm long-range cut-off, a reaction field correction was applied using a relative dielectric constant of ε_r = 78.5. Note that the GROMOS 54A7 forcefield has been specifically parameterised for use with a reaction field and the given cut-off values [28]. The SHAKE algorithm [29] was used to constrain the lengths of the covalent bonds. The SETTLE algorithm [30] was used to constrain the geometry of the water molecules. In order to extend the timescale that could be simulated, explicit hydrogen atoms in the protein were replaced with dummy atoms, the positions of which were calculated at each step based on the positions of the heavy atoms to which they were attached. This eliminates high frequency degrees of freedom associated with the bond-angle vibrations involving hydrogen atoms, allowing a time step of 4 fs to be used to integrate the equations of motion without affecting thermodynamic properties of the system significantly [31]. The simulations were carried out in the NPT ensemble at T = 300 K and P = 1 bar. The temperature and pressure were maintained close to the reference values by weakly coupling the system to an external temperature and pressure bath using a relaxation time constant of

0.1 ps and 0.5 ps, respectively. The compressibility was 4.5×10^{-5} bar and the pressure coupling was isotropic. Configurations were saved every 40 ps for analysis. Images of the protein were produced using VMD .

For simulations of wild-type PsaA, the metal-free PsaA crystal structure was placed in a box of SPC water. As the primary sequence of wild-type PsaA has a net charge of -10 *e*, 10 Na^+ counter-ions were added to ensure the overall charge neutrality of the system. Further ions were added to adjust the concentration of the solution to 200 mM NaCl. Three independent sets of 50 ns unrestrained MD simulations were performed. The end structures from the wild-type PsaA simulations were used as the starting structures for the simulations of spin-labelled Cys-PsaA variants. A single point mutation of cysteine covalently bound to the MTSL probe was incorporated into each of the PsaA systems, at residues L56, S58, I125, I236 and S266, as shown in Figure 1. The MTSL spin label was parameterized using the Automated Topology Builder (ATB) as described previously [34]. The optimised geometry and the topology for the MTSL is available from the ATB webserver [33]. Each PsaA variant underwent 1000 steps of energy minimization using a steepest descent algorithm, followed by 0.5 ns of unrestrained MD simulation to allow the conformation of the cysteine-linked spin-label to respond to the local environment of the protein. Each of the five PsaA variants was solvated in a box of SPC water and Na^+ counter-ions were added to ensure the overall charge neutrality of the system. Further ions were added to adjust the concentration of the solution to 200 mM NaCl. For each of the five MTSL-labelled PsaA systems (referred to as L56C, S58C, I125C, I236C and S266C), three independent sets of 300 ns unrestrained MD simulations were performed.

Analysis of MD simulations

Cluster analysis of wild-type and variant PsaA: The trajectories from all independent simulations of the wild-type PsaA and the five MTSL-labelled Cys-PsaA variants were concatenated to a single trajectory containing 840 structures from PsaA variant simulations and 80 structures from wild-type

PsaA simulations. Cluster analysis was preformed on the backbone structure of the PsaA protein using the clustering algorithm described by Daura and co-workers [35], using cut-offs between 0.1 nm and 0.3 nm. In this work, two conformations were considered to fall within the same cluster if the backbone RMSD between the conformations was less than the specified cut-off.

Root mean squared deviation (RMSD): As a measure of the difference between configurations extracted from the trajectories or clusters, the RMSD was calculated using the method of Maiorov and Crippin[36] after first performing a rotational and translational fit of each frame of the trajectory to a reference structure or domain.

Orientation and rotational mobility of the MTSL label: For each of the five MTSL-labelled PsaA variants, the trajectories from the 3 independent runs were combined. To remove rotational and translational motion from the system, the protein was aligned to the starting structure using all backbone atoms except atoms in the spin label. To estimate the motion of the MTSL spin label its Root Mean Square Fluctuation (RMSF) was calculated for each of the five MTSL-labelled PsaA variants. The RMSF value was calculated using all non-hydrogen atoms in the MTSL molecule and averaged over all frames in the respective trajectory. To de-couple the motion of the spin label from the conformational changes of the protein, the rotational angle of the probe relative to the Cα of the covalently bound cysteine was calculated. For this, the vector between the MTSL pyrrole nitrogen and the Cα of the covalently bound cysteine was calculated as a function of simulation time and the rotational angle of the probe was then calculated as the arccosine of the vector dot product, as described previously [34]. For each of the five MTSL-labelled PsaA variants, the time-dependent data of the rotational angle was binned into histograms and plotted as radial plots. Volumetric maps prepared in VMD showing the occupancy of probe throughout the simulation were used to visualize the mobility of the probe in the different PsaA variants.

Flexibility of the PsaA protein: The mobility of the different domains in the PsaA protein was determined by calculating the RMSF of the Cα of each residue in PsaA. The RMSF was calculated

using a trajectory containing 840 structures from PsaA variant simulations and 80 structures from wild-type PsaA simulations and the RMSF values were averaged over all atoms in each residue to a single RMSF value per residue.

RESULTS

Cys-PsaA variants interact with Mn^{2+} in vitro

PsaA has a single metal-binding site located ~1.5 nm beneath the solvent accessible surface of the protein (Figure 1a), which is able to bind ~1 mol of Mn^{2+} per mol of protein [23, 37]. As shown in Figure 1, the cysteine substitutions used for MTSL spin-labelling are located outside of the metal binding site; nevertheless an equilibrium-binding assay was used to verify that incorporation of the point mutations did not affect Mn^2 -binding. We observed that the metal-free variants showed Mn^{2+} binding comparable to wild-type PsaA (Table 1), indicating that the cysteine substitutions had not altered the metal-receptor properties of PsaA. Therefore, it can be inferred that the metal-free Cys-PsaA variants adopted a tertiary structure that was compatible with metal-ion interaction equivalent to the wild-type protein [23].

Cys-PsaA variants are structurally equivalent to wild-type PsaA

Unrestrained MD simulations of metal-free wild-type PsaA and the five metal-free MTSL-labelled Cys-PsaA variants (each incorporating a single point mutation) were carried out. For the wild-type PsaA, three independent sets of simulations were performed, each lasting 50 ns, giving a combined simulation time of 150 ns. For each of the five MTSL-labelled Cys-PsaA variants, three independent sets of 300 ns simulations were performed, giving a combined simulation time of 900 ns for each variant. Thus in total, 4.65 μs of unrestrained MD simulations of metal-free PsaA were carried out. The longer simulation time of the spin-labelled Cys-PsaA variants was to ensure sufficient sampling of the MTSL spin label.

Table 1. *Binding of Mn^{2+} by metal-free wild-type PsaA and Cys-PsaA variant proteins.*

Sample	Molar Ratio (Mn^{2+}:PsaA)[a]
PsaA 10:1 Mn^{2+}	0.92 ± 0.05
L56C-PsaA 10:1 Mn^{2+}	0.78 ± 0.06
S58C-PsaA 10:1 Mn^{2+}	0.84 ± 0.05
I125C-PsaA 10:1 Mn^{2+}	0.81 ± 0.08
I236C-PsaA 10:1 Mn^{2+}	0.91 ± 0.23
S266C-PsaA 10:1 Mn^{2+}	0.80 ± 0.10

[a] Values shown represent the average and standard deviation from at least 3 independent measurements.

To further ensure that the incorporation of MTSL-labelled cysteine has not resulted in large structural changes of metal-free PsaA a cluster analysis [35] was performed. For this, the trajectories from simulations of wild-type PsaA and all five MTSL-labelled Cys-PsaA variants were combined into a single data set. Using a backbone Root Mean Square Deviation (RMSD) cut-off of 0.30 nm, all structures from simulations of the five PsaA variants and the wild-type PsaA were grouped into a single cluster, showing that within this cut-off, the mutant variants and wild-type PsaA can be considered as structurally equivalent. Note that two structures from a protein of between 200 and 300 amino acids in length that show a backbone RMSD of 0.30 nm can be considered similar and indicates the absence of large structural rearrangements [38, 39]. Collectively, the cluster analysis and the metal-binding assays confirmed that introducing a cysteine and labelling with MTSL does not perturb the overall structure of the protein and that the Cys-PsaA variants can be considered functionally and structurally equivalent to wild-type PsaA in solution.

Conformational dynamics of metal-free PsaA in solution

To investigate the conformational dynamics of metal-free PsaA in solution, the cluster analysis of the combined trajectory was repeated using progressively smaller cut-offs. Analysis with a 0.25 nm RMSD cut-off identified 13 clusters, of which 11 contained 2 or more structures. These clusters capture the most frequently occurring localized motions of metal-free PsaA in solution. Repeating the cluster analysis with lower cut-offs produced more clusters, but did not identify any additional subpopulations with distinct structural features. Figure 2 shows the assignment of structures from the combined trajectory to the four main clusters and also illustrates the characteristic motions that distinguish the structures in each cluster.

The four most populated clusters contained 82% (cluster 1), 5% (cluster 2), 4% (cluster 3) and 3% (cluster 4) of the conformations, representing 94% of the combined trajectories. The assignment of structures to the full set of clusters can be found in Supplementary Figure S1. It is important to note that structures from both wild-type and all five Cys-PsaA variants are found in the dominant cluster (cluster 1) and that structures from WT simulations are also found in most of the other clusters (see also Supplementary Figure S1). Further analysis showed that clusters 1 and 3 contained 55% and 17.5% of the 80 structures from simulation wild type PsaA, respectively. The remainder of the wild type conformations were distributed across 4 more clusters. This further confirms that WT and Cys-PsaA variants can be considered structurally equivalent and that the mutations and introduction of the spin label did not results in significantly increased sampling of conformations that are not present in the wild-type protein.

The most populated cluster, cluster 1 in Figure 2, represents the major PsaA conformation. Here the orientations of the N- and C-terminal lobes were found in positions analogous to that of the metal-free PsaA crystal structure (PDB ID 3ZK7). The backbone RMSD between the central conformation of cluster 1 and that of the solvated PsaA crystal structure used to initiate the simulations is 0.17 nm. As can be seen in Figure 2, clusters 2, 3 and 4 represent conformations in

which there was a lateral splaying of the C-terminal lobe, characterized by an outward motion of the P4 domain (residues 250 – 280, orange) and the 'mobile helix' (residues 220 – 250, red) away from the longitudinal axis of the protein. This motion is accompanied by an increased mobility of the loop adjacent to the metal-binding site (residues 120 – 130, purple). The relative extent of these motions is the main difference between the conformations of clusters 2, 3 and 4. It should be noted that the distribution of the backbone RMSD of PsaA conformations identified lay within a 0.3 nm cut-off and are consistent with the RMSDs previously reported by Couñago et al. [23]. From the structures in each of the 4 most dominant clusters seen in Figure 2, it is evident that the C-terminal lobe of PsaA exhibits the highest conformational fluctuations. Further analysis of the concatenated trajectories showed that the splaying of the C-terminal lobe is reversible, and that there is inter-conversion between the conformations of the structures found in the four dominant clusters, as can be seen in the cluster assignment in Figure 2 and Figure S1 in the Supplementary Material, as well as Figure S2 that illustrates the transitions between clusters.

To quantify the relative flexibility of the different structural domains of metal-free PsaA, the per-residue Root Mean Square Fluctuation (RMSF) was calculated using the combined trajectory. Figure 3a shows the per-residue RMSF with regions of high, intermediate and low RMSF values shaded in red, orange and blue, respectively. The protein domains that correspond to these regions are shown in the same colours in Figure 3b. The linking helix that connects the C- and N-terminal lobes (residues 150-220) showed the lowest RMSF values with a slight increase in mobility towards the C-terminal half. The P4 domain in the C-terminal lobe (residues 250-280) and the two helix-loop domains in the N-terminal lobe (residues 50-75 and 90-110) showed intermediate RMSF values. The regions of highest mobility were the short loop between the C- and N-terminal lobes (residues 120-130) and the helix-loop domain of the C-terminal lobe preceding the antigenic P4 region (the mobile helix).

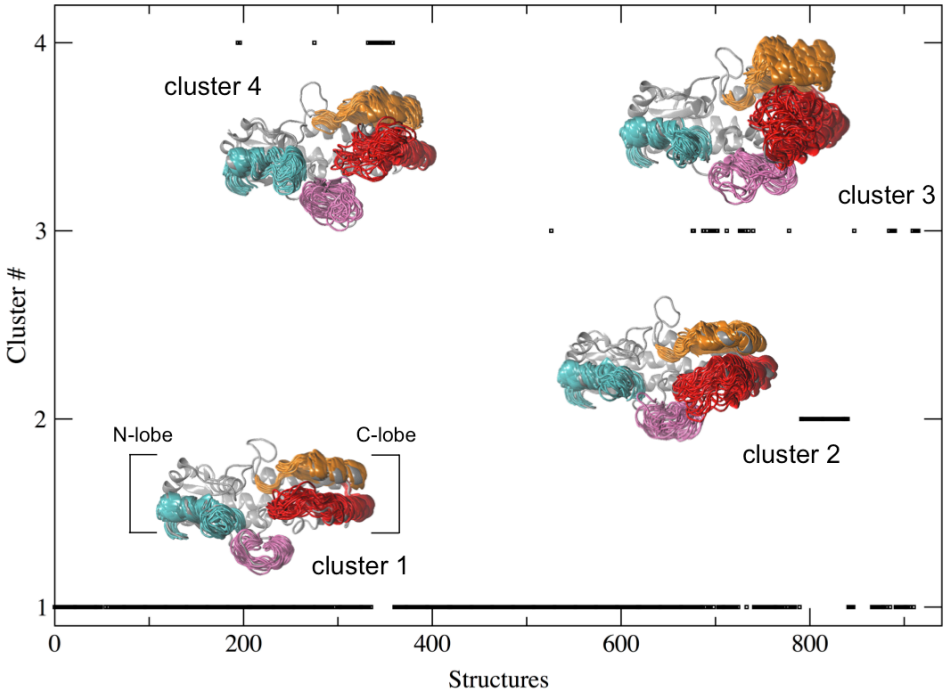

Figure 2. *Clustering of PsaA structures in solution. 840 structures from simulations of the five Cys-PsaA variants and 80 structures from simulations of wild-type PsaA were combined and clustered using a 0.25 nm cut-off. The 4 largest clusters, containing 94% of all structures, are shown. The N-terminal helix is shown in cyan. The mobile helix and P4 domain in the C-terminal lobe are shown in orange and red, respectively. The loop adjacent to the metal binding site is shown in purple.*

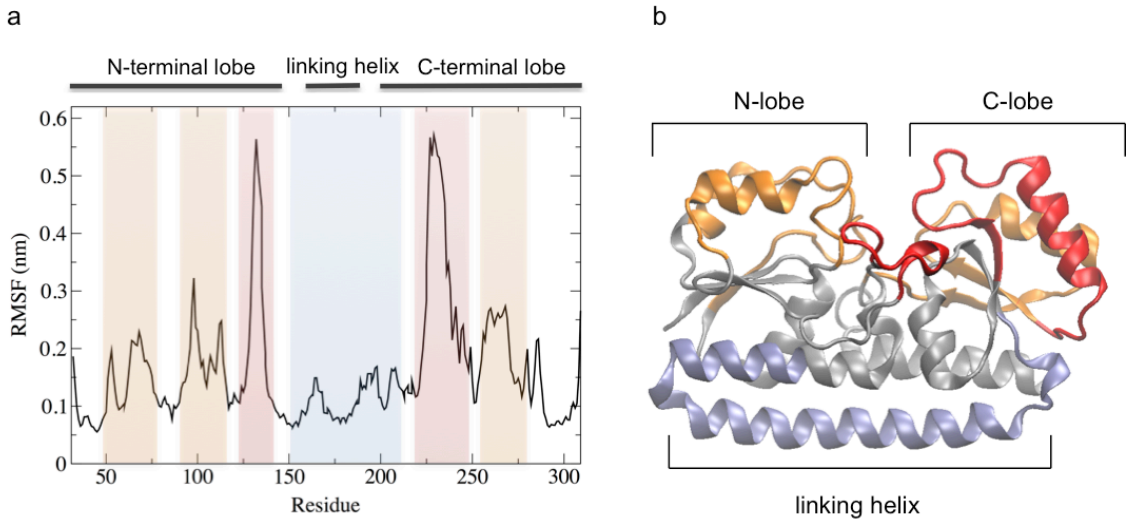

Figure 3. *Flexibility of structural domains of metal-free PsaA in solution. Per-residue RMSF calculated from MD simulations of metal-free wild-type and Cys-PsaA mutant variants. Regions with the highest, intermediate and lowest RMSF values are highlighted in red, orange and blue, respectively (a). Structure of the metal-free PsaA protein showing domains with the highest (red), intermediate (orange) and lowest mobility (blue) based on RMSF values (b).*

Given that the lateral splaying of the C-terminal lobe and the loop flanking the metal binding site was observed in many of the conformations of PsaA in solution, a more detailed structural analysis of the metal binding residues in the PsaA crystal structures and the solution model was carried out. Comparison of the metal binding residues, His67, His139, Glu205 and Asp280, in the Mn-bound and metal-free PsaA crystal structures showed that these residues are further apart in the absence of the metal ion [23]. In the simulations of metal-free PsaA in solution, the inter-residue distance between His67 and Glu205 was significantly larger than observed in the metal-free crystal structure (see Supplementary Figure S3 and Supplementary Table S3). A similar increase was observed in the simulations reported by Couñago *et al.* [23]. Furthermore, it is notable that the partial unwinding of the linking helix observed crystallographically on metal binding [23] was not sampled in any of the conformations from the MD simulations.

Mobility of protein domains based on EPR spectroscopy

To complement the MD simulations, the cw EPR spectra for the five MTSL-labelled Cys-PsaA variants were collected. The spectral line-shapes, shown in Figure 4, provide information about the motion of the spin-label on the picosecond (ps) to microsecond (μs) time scale and are a result of the paramagnetic relaxation of the MTSL spin-label. Fast protein backbone motion on the nanosecond (ns) time scale can also affect the line-shape. The characteristic MTSL spectrum arises from interaction of the unpaired electron with the nitroxide ^{14}N nucleus (nuclear spin, I = 1) to give three dominant spectral features that correspond to hyperfine coupling in the m_I (0, ±1) states. The detailed spectral line-shape of MTSL is dependent on the mobility of the nitroxide spin-label. A very sharp EPR line-shape is characteristic of a highly mobile spin-label with fast inter-conversion between the different rotameric states, while peak broadening results from immobilized labels with slow or no inter-conversion between states. Thus, the comparison of line-shapes and the relative peak broadening in the spectra can be used to calculate the relative mobility of the MTSL attached to different parts of the PsaA protein. Typical reorientational correlation times (τ_c) are <1 ns for highly mobile, > 4 ns for slow tumbling and approaching 1 μs for immobilised nitroxide spin-labels. As motion becomes faster, exchange between spin-label orientations leads to averaging of the anisotropic hyperfine contributions to the line-shape of the spectrum[40]. The outer extrema hyperfine splitting in the nitroxide spectrum, anisotropic at the rigid limit ($2A_{zz}' \approx 6.8$ mT), become narrower as they become isotropic in highly mobile spin-labels ($2A_{zz}' = 2A_{iso} \approx 3.0$ mT) (shown in Figure 4).

The 5 MTSL-labelled Cys-PsaA variants gave X-band EPR spectra that are typical for spin-labelled proteins with τ_c varying between ~1 to 10 ns. EPR simulations of the spectra were performed, under the assumption of isotropic rotational motion of MTSL, to obtain τ_c, for the motion of the nitroxide spin-label of each of the PsaA variants (Figure 4, dotted lines). The EPR spectrum of the S266C variant, located within the antigenic P4 region of PsaA, showed the sharpest line-shape, indicating the label was highly mobile with a τ_c of 970 ps (Figure 4e). By contrast, the L56C

(Figure 4a) and S58C variants (Figure 4b) variants, from the N-terminal domain, and the I236C variant (Figure 4c) isoform, from the C-terminal domain, showed extensive peak broadening, concordant with slow spin-label tumbling and τ_c s of 7-10 ns. The spectrum of the I236C variant also showed the presence of a small percentage (13 %) of more mobile spin-label (τ_c of 1.2 ns). The I125C variant showed only some broadening with a τ_c of 2.7 ns (Figure 4d) indicative of intermediate mobility. Collectively, the results from the cw EPR spectroscopy experiments showed an order of relative mobility, from least to greatest, of: S58C < L56C < I236C (87% of spin-label) < I125C < S266C ≈ I236C (13 % of spin-label) (Figures 4 a-e).

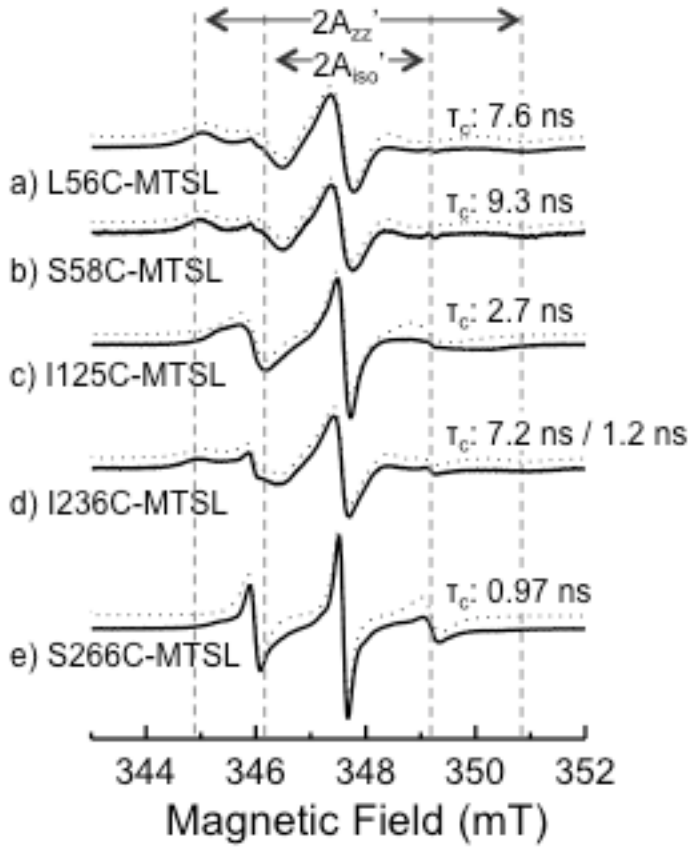

Figure 4. *Representative cw EPR spectra of the five Cys-PsaA variants in which a MTSL label was introduced at positions a) L56, b) S58, c) I125, d) I236 and e) S266. Simulations were performed using Easyspin*[24] *and are shown as dotted lines with* τ_c *indicated. The spectra of the L56C, S58C, I125C and S266C PsaA variants were simulated using a single component, whereas the spectrum of the I236C PsaA variant required simulation with two components. For the two-component simulation of d) I236C, the* τ_c *of both components is given and the weighting is 87 % to 13 % for each. Vertical lines are shown to indicate peak broadening. 2Aiso' ≈ 3 mT and 2Azz' ≈ 6.8 mT show the two extremes of hyperfine splitting when motionally averaged with high spin-label mobility and at the rigid limit, respectively.*

Mobility of spin-labels from MD simulations

MD simulation techniques enable the tracking of spin-label motion with atomic resolution in the ps to ns timescales. As the temporal resolution of MD simulations corresponds to those of EPR spectroscopy, they can provide a complementary means of examining both the motion and local environment of the paramagnetic probe [41-44]. MD simulations are increasingly used to aid in the interpretation and analysis of EPR data, as it enables the de-convolution of probe motion from the underlying motion of the protein [41-48]. It is important to note that the comparison between spin mobility form MD simulations and the line shapes from the cw EPR spectra were compared on a qualitative basis. The mobility of the spin-labels for the 5 MTSL-labelled Cys-PsaA variants was first estimated by calculating the RMSF of the incorporated MTSL-cysteine for each point mutation in PsaA (Figure 5). For this, the protein was aligned to its starting structure to remove the rotational and translational motion of the entire system. The RMSF was then calculated using all non-hydrogen atoms in the Cys-MTSL and averaged over all frames in the simulation of the respective Cys-PsaA variant. Therefore, the RMSF provides a measure of the deviation of the cysteine-linked MTSL spin-label from its initial position, as the simulation evolves over time. The RMSF values indicate that the spin labels attached to residues in the N-terminal lobe (L56 and S58) are significantly less mobile than the ones attached to residues in the C-terminal lobe (I236 and S266) or the loop flanking the metal binding site (I125). To visualize the relative mobility of the five spin-labels, volumetric maps based on the occupancy of the Cys-MTSL label over the entire simulation were generated (see Supplementary Figure S4).

While the time-averaged RMSF provides information on the relative mobility of the probe in the different Cys-PsaA variants, it does not report on the probe's rotational motion. This was calculated as the rotational angle of the probe relative to the C α of the covalently bound cysteine after again removing the rotational and translational motion of the system. This captures the rotational motion of the spin label independent of the underlying motion of the protein. Figure 6 shows the radial distribution plots of the rotational angles for each variant. The data shows that L56C-MTSL

samples a very narrow rotational motion in comparison to the other variants. It also exhibited the lowest RMSF of all the Cys-MTSL probes and produced a high degree of spectral broadening in EPR (T_c = 7.6 ns), indicating that L56C-MTSL is highly immobilized. This is explained by its local environment. L56 is located in the β-sheet region of the N-terminal $(\beta/\alpha)_4$-domain, consisting of four parallel β-strands. The β-sheet hydrogen-bonding network between the backbone carbonyl and amide groups of residues Val35, Ala37, Asp55, His57 and Ile59 constrain the L56C-MTSL backbone to the plane of the β-sheet. The side chain of L56C-MTSL is sterically constrained by the side chains of Lys47 and Asp52, which severely restricts its rotational motion.

a

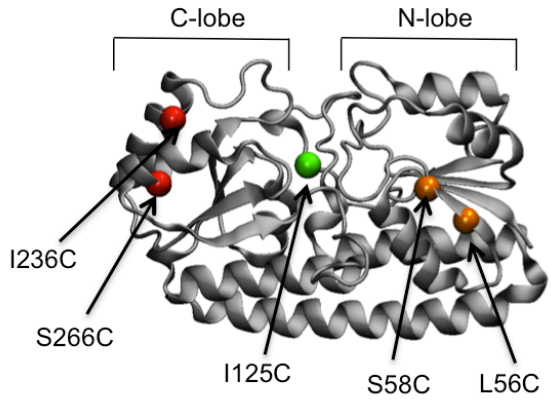

b

RMSF for the MTSL label in the five Cys-PsaA variants

PsaA Isoform	RMSF ± 1 stdev
L56C-PsaA	0.06 ± 0.01
S58C-PsaA	0.09 ± 0.01
I125C-PsaA	0.12 ± 0.01
I236C-PsaA	0.14 ± 0.01
S266C-PsaA	0.14 ± 0.01

Figure 5. *Relative mobility of MTSL labels. MTSL labels are coloured by relative mobility based on MD simulations; least mobile in orange (L56C and S58C), intermediate mobility in green (I125C), most mobile in red (S266C and I236C) (a). The RMSF values for the MTSL spin labels in each of the five Cys-PsaA variants was calculated using all non-hydrogen atoms in the MTSL molecule and was averaged over all frames in the simulation (b).*

The bimodal distribution for S58C-MTSL suggests the spin-label at this position has two preferred orientations, both with low mobility. The mobility of S58C-MTSL is comparable to that of the L56C-MTSL spin-label, in agreement with the peak broadening in the EPR spectra (T_c = 9.3 ns ,

Figure 4). S58C-MTSL is located within the same N-terminal β-sheet region, two residues away from L56C, but has higher solvent accessibility. The backbone mobility of S58C-MTSL is again constrained by the rigid β-sheet motif. However, the S58C-MTSL side chain has a greater degree of mobility and switches between a preferred orientation, in which the MTSL nitroxide oxygen interacts with the primary amine of Lys47, and a second more mobile orientation that lacks specific interactions. The low RMSF of S58C-MTSL suggests that there is only a slow interchange between the two preferred angular rotations.

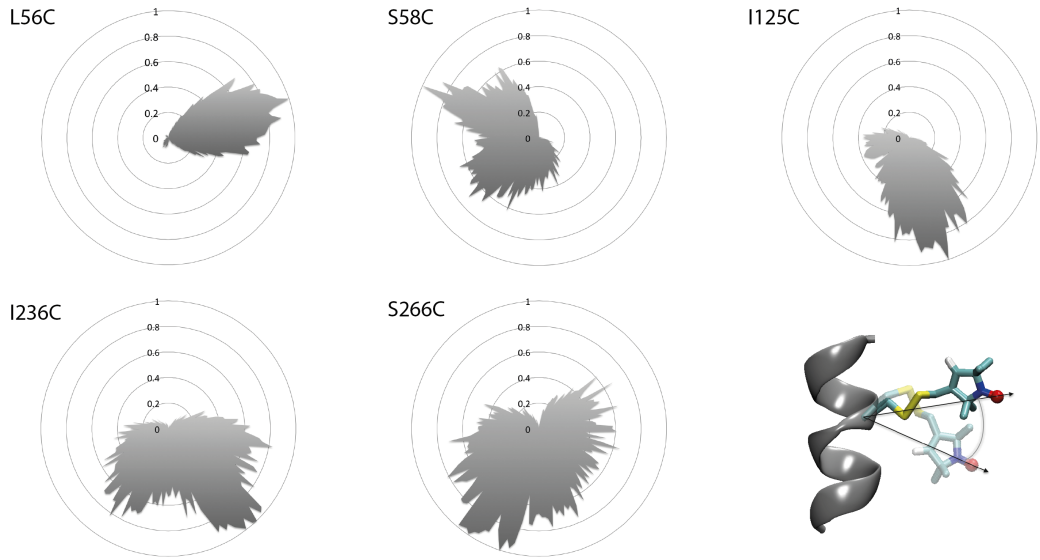

Figure 6. *Radial distribution plots of histograms for the rotational angle of the MTSL spin-label in the five Cys-PsaA variants. The rotational motion of the spin-label is estimated by the distribution of the rotational angle of the vector between the MTSL pyrrole nitrogen and the Cα of the cysteine.*

The radial distribution of the I125C-MTSL, along with its RMSF value, suggests an intermediate mobility, albeit lower than expected from the EPR spectra. I125C-MTSL is located in the extended loop region flanking the metal-binding site. The I125C-MTSL backbone carbonyl forms a β-sheet hydrogen bond with the backbone amide of Asp137. The short stretch of β-sheet is also H-bonded between the backbone amide of Leu96 and backbone carboxyl of Lys104. Further interactions

between the side chains of Asp137 and Tyr210 (in the C-terminal lobe) contribute to the coordination of this region of the protein.

I236C-MTSL and S266C-MTSL, both of which are located in the C-terminal domain, show very broad angular distributions and high RMSF values, indicating these labels have increased mobility compared to labels in other domains of the protein. In the MD simulations, both I236C-MTSL and S266C-MTSL are highly solvent-accessible and do not form any stable contacts with surrounding residues. Consequently, these labels are not restricted in their mobility. In particular, S266 shows very broad radial distribution suggesting almost complete free rotational motion, consistent with the sharp peaks in the EPR spectra. The peak broadening in the EPR spectra of I236C-MTSL suggests lower mobility than indicated by the MD simulations. Overall, the RMSF values and the rotational motion analyses indicate a relative mobility profile, from least to greatest, of: L56C < S58C < I125C < I236C ≈ S266C. Collectively, based on the qualitative comparison o the spin mobility and peak broadening, the cw EPR and MD simulations showed acceptable agreement in the prediction of relative mobility for the restricted (L56C, S58C) and very mobile (I236C, S266C) labels.

DISCUSSION

PsaA is a part of the primary Mn^{2+} uptake pathway of *S. pneumoniae*, and facilitates the acquisition of this essential trace element from the extracellular environment. Our recent studies have also shown that PsaA has a vital role in *S. pneumoniae* virulence [4-6], and blocking PsaA with zinc or cadmium, impairs bacterial growth due to disruption of Mn^{2+} acquisition [37, 49]. Understanding the molecular details that underpin the PsaA-facilitated process of metal-binding and subsequent release is fundamental to expanding our knowledge of *S. pneumoniae* virulence and, more generally, the acquisition of essential transition metal ions at the host-pathogen interface. The crystal structures of the metal-free and metal-bound PsaA were a first step towards understanding the metal binding, indicating that the C-terminal domain of PsaA undergoes a rigid body motion of the C-terminal domain via a "spring-hammer" mechanism to facilitate metal binding [23]. However,

these crystal structures only provide static snapshots of the most stable conformations and cannot provide information on the conformational dynamics of proteins in solution. Thus, the aim of this study was to characterize the conformational flexibility of metal-free PsaA in solution using a combination of MD simulations and cw EPR spectroscopy. For this, five Cys-PsaA variants that were labelled with the spin-label MTSL at positions L56, S58, I125, I236 and S266 were used to collect cw EPR spectra and the relative mobility of the spin-labels in the five variants was determined from the EPR spectra as well as from MD simulations. In addition, a cluster analysis on the structures from the MD simulations was used to find the most common conformations that PsaA adopts in solution in the absence of a metal ion.

The results from the MD simulations and the cw EPR experiments clearly indicate that the C-terminal lobe is more flexible than the N-terminal lobe. The per-residue RMSF further showed that the C-terminal helical residues 220 to 250, referred to, as the “mobile helix”, and the loop flanking the metal binding site are the most flexible regions of the protein, while the linking helix is the most structurally rigid domain. This result is consistent with prior structural observations [17, 23, 37]. The flexibility of the mobile helix is notable, as it contains the negatively charged residues predicted to be essential for recognition by the transmembrane domain of the ABC transporter, PsaC. It is important to note that the secondary structure of the mobile helix is always maintained in simulations, while its orientation with respect to the rest of the protein varies, increasing the conformational states sampled by PsaA in solution. Thus, we hypothesise that the increased flexibility and variability in orientation of this region of PsaA could act as a mechanism by which to abrogate potential non-productive interaction with PsaC in the absence of the metal-loaded form of the SBP. The results from the cw EPR line shapes show reasonable agreement with the relative mobility from MD simulations, except for the case of I236C in the flexible C-terminal domain. The complex line shape of I236C suggests a dynamic conformational exchange between two states that are related to each other by the outward movement of the C-terminal lobe. The major rotamer is less mobile than predicted by the MD simulations and has a characteristic broad line shape that suggests

the motion of the MTSL nitroxide is restricted by the C-terminal helix. Rotation of the C-terminal helix increases the relative mobility of the nitroxide, producing a sharp spectral cw EPR line shape, as seen in the MD simulations. The two components are proportional to the frequency of sampling of each respective population, which differs in the MD and the cw EPR, likely due to insufficient statistics on the relative occurrences of the two states in the MD simulations.

The results from the clustering analysis of the MD simulations indicate that the crystal structure of metal-free PsaA provides an accurate representation of the dominant conformation of metal-free PsaA in solution. However, the analysis also revealed a number of conformational sub-populations that show a lateral splaying of the C-terminal lobe through increased movements of the antigenic P4 domain, the mobile helix and the small loop connecting the C- and N-terminal lobes. These conformations represent a smaller yet distinctly different component of the conformational landscape of metal-free PsaA protein in solution that is not captured by the crystal structure. Analysis of inter-residue distances suggests that the metal binding site is larger and more solvent exposed than indicated by the crystals structure and previous MD simulations [23], increasing the accessibility of the metal binding site for metal loading and delivery to the PsaC permease. During the combined 4.65 μs of unrestrained simulations, the distance between these residues never approached distances short enough to capture a metal ion. Collectively, this indicates in the absence of metal ions, PsaA does not dynamically sample the metal-bound crystallographic conformation required for binding and recognition by the PsaBC ABC transporter complex [23]. This is consistent with the previous simulations reported by Couñago *et al*., where it was observed that PsaA rapidly diverged from the metal-bound crystallographic conformation on removal of the bound metal-ion. Overall, the flexibility and the conformational dynamics of metal-free PsaA in solution revealed in this study are consistent with the rigid-body movements observed in the transition from the metal-free to the metal-bound structural conformations, *i.e.* the spring-hammer ligand-binding mechanism [23]. This work provides new atomic-resolution insights into the conformational flexibility of prokaryotic metal-receptor proteins and the importance of specific domains within the cluster A-I

SBP PsaA. Furthermore, these findings lay the groundwork for future EPR and MD based studies of metal-receptor proteins in *S. pneumoniae* and other prokaryotes.

ACKNOWLEDGMENTS

This research was undertaken with the assistance of resources provided at the NCI National Facility systems at the Australian National University through the National Computational Merit Allocation Scheme supported by the Australian Government. We thank Dr R.M. Couñago for his insights and discussions. This work was supported by the Australian Research Council (ARC) grants [DP120103957, DP150104515] to C.A.M. and J.C.P., the National Health & Medical Research Council (NHMRC) grants; [1022240, 1080784] to C.A.M., and [565526, 1071659] to J.C.P. and B.K., and the Medical Advances without Animal Trust (MAWA) to E.D. and M.L.O. The author(s) declare no competing financial interests. M.L.O. holds an ARC DECRA [DE120101550]. B.K. is a NHMRC Senior Research Fellow. J.C.P. is a NHMRC Senior Principal Research Fellow. E.D. is a NHMRC ECR Fellow and part of the work was carried out while she was on a Fellowship of the Swiss National Science Foundation.

AUTHOR CONTRIBUTIONS

S.L.B., R.C. and C.A.M. designed and executed all the biochemical studies. E.D. and M.L.O. designed and executed the molecular dynamics experiments. J.H.V. and F.M designed and executed the EPR studies. E.D., M.L.O, C.A.M. S.L.B., J.H.V. drafted the manuscript. All authors contributed to the design, analysis, discussion of the research, and writing and editing of the final manuscript.

REFERENCES

1. Ma, Z.; Jacobsen, F. E.; Giedroc, D. P., Coordination chemistry of bacterial metal transport and sensing. *Chem Rev* **2009,** *109* (10), 4644-4681.
2. Waldron, K. J.; Rutherford, J. C.; Ford, D.; Robinson, N. J., Metalloproteins and metal sensing. *Nature* **2009,** *460* (7257), 823-830.
3. Dintilhac, A.; Alloing, G.; Granadel, C.; Claverys, J. P., Competence and virulence of *Streptococcus pneumoniae*: Adc and PsaA mutants exhibit a requirement for Zn and Mn resulting from inactivation of putative ABC metal permeases. *Mol Microbiol* **1997,** *25* (4), 727-739.
4. McAllister, L. J.; Tseng, H.-J.; Ogunniyi, A. D.; Jennings, M. P.; McEwan, A. G.; Paton, J. C., Molecular analysis of the *psa* permease complex of *Streptococcus pneumoniae*. *Mol Microbiol* **2004,** *53* (3), 889-901.
5. Berry, A. M.; Paton, J. C., Sequence heterogeneity of PsaA, a 37-kilodalton putative adhesin essential for virulence of *Streptococcus pneumoniae*. *Infect Immun* **1996,** *64* (12), 5255-5262.
6. Marra, A.; Lawson, S.; Asundi, J. S.; Brigham, D.; Hromockyj, A. E., *In vivo* characterization of the *psa* genes from *Streptococcus pneumoniae* in multiple models of infection. *Microbiology* **2002,** *148* (Pt 5), 1483-91.
7. Ogunniyi, A. D.; Mahdi, L. K.; Jennings, M. P.; McEwan, A. G.; McDevitt, C. A.; Van der Hoek, M. B.; Bagley, C. J.; Hoffmann, P.; Gould, K. A.; Paton, J. C., Central role of manganese in regulation of stress responses, physiology, and metabolism in *Streptococcus pneumoniae*. *J Bacteriol* **2010,** *192* (17), 4489-4497.
8. Papp-Wallace, K.; Maguire, M., Manganese transport and the role of manganese in virulence. *Annu Rev Microbiol* **2006,** *60*, 187-209.
9. Rajam, G.; Phillips, D. J.; White, E.; Anderton, J.; Hooper, C. W.; Sampson, J. S.; Carlone, G. M.; Ades, E. W.; Romero-Steiner, S., A functional epitope of the pneumococcal surface adhesin A activates nasopharyngeal cells and increases bacterial internalization. *Microb Pathog* **2008,** *44* (3), 186-96.
10. Rajam, G.; Skinner, J.; Melnick, N.; Martinez, J.; Carlone, G. M.; Sampson, J. S.; Ades, E. W., A 28-aa pneumococcal surface adhesin A-derived peptide, P4, augments passive immunotherapy and rescues mice from fatal pneumococcal infection. *J Infect Dis* **2009,** *199* (8), 1233-8.
11. Bangert, M.; Bricio-Moreno, L.; Gore, S.; Rajam, G.; Ades, E. W.; Gordon, S. B.; Kadioglu, A., P4-mediated antibody therapy in an acute model of invasive pneumococcal disease. *J Infect Dis* **2012,** *205* (9), 1399-407.
12. Romero-Steiner, S.; Caba, J.; Rajam, G.; Langley, T.; Floyd, A.; Johnson, S. E.; Sampson, J. S.; Carlone, G. M.; Ades, E., Adherence of recombinant pneumococcal surface adhesin A (rPsaA)-coated particles to human nasopharyngeal epithelial cells for the evaluation of anti-PsaA functional antibodies. *Vaccine* **2006,** *24* (16), 3224-31.
13. Weeks, J. N.; Boyd, K. L.; Rajam, G.; Ades, E. W.; McCullers, J. A., Immunotherapy with a combination of intravenous immune globulin and p4 peptide rescues mice from postinfluenza pneumococcal pneumonia. *Antimicrob Agents Chemother* **2011,** *55* (5), 2276-81.
14. Bangert, M.; Wright, A. K.; Rylance, J.; Kelly, M. J.; Wright, A. D.; Carlone, G. M.; Sampson, J. S.; Rajam, G.; Ades, E. W.; Kadioglu, A.; Gordon, S. B., Immunoactivating peptide p4 augments alveolar macrophage phagocytosis in two diverse human populations. *Antimicrob Agents Chemother* **2013,** *57* (9), 4566-9.
15. WHO *World Health Organization position paper: pneumococcal vaccines* World Health Organization: 2012; pp 129-144.
16. Counago, R. M.; McDevitt, C. A.; Ween, M. P.; Kobe, B., Prokaryotic substrate-binding proteins as targets for antimicrobial therapies. *Curr Drug Targets* **2012,** *13* (11), 1400-10.

17. Lawrence, M. C.; Pilling, P. A.; Epa, V. C.; Berry, A. M.; Ogunniyi, D. A.; Paton, J. C., The crystal structure of pneumococcal surface antigen PsaA reveals a metal-binding site and a novel structure for a putative ABC-type binding protein. *Structure* **1998,** *6*, 1553–1561.
18. McDevitt, C. A.; Ogunniyi, A. D.; Valkov, E.; Lawrence, M. C.; Kobe, B.; McEwan, A. G.; Paton, J. C., A molecular mechanism for bacterial susceptibility to zinc. *PLoS Pathogens* **2011,** *7*, e1002357.
19. Berntsson, R. P.; Smits, S. H.; Schmitt, L.; Slotboom, D. J.; Poolman, B., A structural classification of substrate-binding proteins. *FEBS Lett* **2010,** *584* (12), 2606-17.
20. Woo, J. S.; Zeltina, A.; Goetz, B. A.; Locher, K. P., X-ray structure of the *Yersinia pestis* heme transporter HmuUV. *Nat Struct Mol Biol* **2012,** *19* (12), 1310-5.
21. Korkhov, V. M.; Mireku, S. A.; Locher, K. P., Structure of AMP-PNP-bound vitamin B12 transporter BtuCD-F. *Nature* **2012,** *490* (7420), 367-72.
22. Felder, C. B.; Graul, R. C.; Lee, A. Y.; Merkle, H. P.; Sadee, W., The Venus flytrap of periplasmic binding proteins: an ancient protein module present in multiple drug receptors. *AAPS PharmSci* **1999,** *1*, 7-26.
23. Counago, R. M.; Ween, M. P.; Begg, S. L.; Bajaj, M.; Zuegg, J.; O'Mara, M. L.; Cooper, M. A.; McEwan, A. G.; Paton, J. C.; Kobe, B.; McDevitt, C. A., Imperfect coordination chemistry facilitates metal ion release in the Psa permease. *Nat Chem Biol* **2014,** *10* (1), 35-41.
24. Stoll, S.; Schweiger, A., EasySpin, a comprehensive software package for spectral simulation and analysis in EPR. *J Magn Reson* **2006,** *178*, 42–55.
25. van der Spoel, D.; Lindahl, E.; Hess, B.; Groenhof, G.; Mark, A. E.; Berendsen, H. J. C., GROMACS: fast, flexible and free *J Comput Chem* **2005,** *26*, 1701-1718.
26. Schmid, N.; Eichenberger, A.; Choutko, A.; Riniker, S.; Winger, M.; Mark, A.; Gunsteren, W., Definition and testing of the GROMOS force-field versions 54A7 and 54B7. *European Biophysics Journal* **2011,** *40*, 843-856.
27. Berendsen, H. J. C.; Postma, J. P. M.; van Gunsteren, W. F.; Hermans, J., Interaction models for water in relation to protein hydration. In *Intermolecular Forces*, Pullman, B., Ed. Springer Netherlands: 1981; Vol. 14, pp 331-342.
28. Schmid, N.; Eichenberger, A.; Choutko, A.; Riniker, S.; Winger, M.; Mark, A.; Gunsteren, W., Definition and testing of the GROMOS force-field versions 54A7 and 54B7. *Eur. Biophys. J.* **2011,** *40* (7), 843-856.
29. Ryckaert, J.-P.; Ciccotti, G.; Berendsen, H. J. C., Numerical integration of the cartesian equations of motion of a system with constraints: molecular dynamics of n-alkanes. *Journal of Computational Physics* **1977,** *23* (3), 327-341.
30. Miyamoto, S.; Kollman, P. A., Settle-analytical version of the shake and Rattle algorithm for rigid water models. *J Comput Chem* **1992,** *13*, 952-962.
31. Feenstra, K. A.; Hess, B.; Berendsen, H. J. C., Improving efficiency of large time-scale molecular dynamics simulations of hydrogen-rich systems. *J Comput Chem* **1999,** *20* (8), 786-798.
32. Humphrey, W.; Dalke, A.; Schulten, K., VMD - Visual Molecular Dynamics. *J Mol Graph Model* **1996,** *14*, 33-38.
33. Malde, A. K.; Zuo, L.; Breeze, M.; Stroet, M.; Poger, D.; Nair, P. C.; Oostenbrink, C.; Mark, A. E., An Automated force field Topology Builder (ATB) and repository: Version 1.0. *J Chem Theory Comput* **2011,** *7* (12), 4026-4037.
34. van Wonderen, J. H.; McMahon, R. M.; O'Mara, M. L.; McDevitt, C. A.; Thomson, A. J.; Kerr, I. D.; MacMillan, F.; Callaghan, R., The central cavity of ABCB1 undergoes alternating access during ATP hydrolysis. *FEBS J* **2014,** *281* (9), 2190-201.
35. Daura, X.; Gademann, K.; Jaun, B.; Seebach, D.; van Gunsteren, W. F.; Mark, A. E., Peptide folding: when simulation meets experiment. *Angew Chem Int Ed* **1999,** *38* (1-2), 236-240.
36. Maiorov, V. N.; Crippen, G. M., Significance of root-mean-square deviation in comparing three-dimensional structures of globular proteins. *J Mol Biol* **1994,** *235* (2), 625-34.

37. McDevitt, C. A.; Ogunniyi, A. D.; Valkov, E.; Lawrence, M. C.; Kobe, B.; McEwan, A. G.; Paton, J. C., A molecular mechanism for bacterial susceptibility to zinc. *PLoS Pathog* **2011,** *7* (11), e1002357.
38. Kandt, C.; Oloo, E. O.; Tieleman, D. P., Domain coupling in the ABC transporter system BtuCD/BtuF: molecular dynamics simulation, normal mode analysis and protein-protein docking. In *21st International Symposium on High Performance Computing Systems and Applications*, 2007; Vol. DOI:10.1109/HPCS.2007.15.
39. Maiorov, V. N.; Crippen, G. M., Significance of Root-Mean-Square Deviation in comparing three-dimensional structures of globular proteins. *J Mol Biol* **1994,** *235* (2), 625-634.
40. Pake, G. E.; Estle, T. L., *The Physical Principles of Electron Paramagnetic Resonance*. W. A. Benjamin University of Minnesota, 1973.
41. Beier, C.; Steinhoff, H.-J., A structure-based simulation approach for alectron paramagnetic resonance spectra using molecular and stochastic dynamics simulations. *Biophys J* **2006,** *91* (7), 2647-2664.
42. DeSensi, S. C.; Rangel, D. P.; Beth, A. H.; Lybrand, T. P.; Hustedt, E. J., Simulation of nitroxide electron paramagnetic resonance spectra from Brownian trajectories and Molecular Dynamics simulations. *Biophys J* **2008,** *94* (10), 3798-3809.
43. Sarver, J. L.; Townsend, J. E.; Rajapakse, G.; Jen-Jacobson, L.; Saxena, S., Simulating the dynamics and orientations of spin-labeled side chains in a protein–DNA complex. *J Phys Chem B* **2012,** *116* (13), 4024-4033.
44. Sezer, D.; Freed, J. H.; Roux, B., Parametrization, Molecular Dynamics simulation, and calculation of electron spin resonance spectra of a nitroxide spin label on a polyalanine α-helix. *J Phys Chem B* **2008,** *112* (18), 5755-5767.
45. Kroncke, B. M.; Horanyi, P. S.; Columbus, L., Structural origins of nitroxide Side chain dynamics on membrane protein α-helical sites. *Biochemistry* **2010,** *49* (47), 10045-10060.
46. Langen, R.; Oh, K. J.; Cascio, D.; Hubbell, W. L., Crystal structures of spin labeled T4 lysozyme mutants: implications for the interpretation of EPR Spectra in terms of structure. *Biochemistry* **2000,** *39* (29), 8396-8405.
47. Oganesyan, V. S., A general approach for prediction of motional EPR spectra from Molecular Dynamics (MD) simulations: application to spin labelled protein. *Phys Chem Chem Phys* **2011,** *13* (10), 4724-4737.
48. Sezer, D.; Freed, J. H.; Roux, B., Multifrequency electron spin resonance spectra of a spin-labeled protein calculated from Molecular Dynamics simulations. *J Am Chem Soc* **2009,** *131* (7), 2597-2605.
49. Begg, S. L.; Eijkelkamp, B. A.; Luo, Z.; Couñago, R. M.; Morey, J. R.; Maher, M. J.; Ong, C.-l. Y.; McEwan, A. G.; Kobe, B.; O'Mara, M. L.; Paton, J. C.; McDevitt, C. A., Dysregulation of transition metal ion homeostasis is the molecular basis for cadmium toxicity in *Streptococcus pneumoniae*. *Nat Commun* **2015,** *6* (6418).